

## Supplementary Materials

### **Boosted thermopower in aqueous thermocells through additives-induced ionic regulation for low-grade heat harvesting**

**Yijie Mu<sup>1</sup>, Kedi Li<sup>2</sup>, Kaiyu Mu<sup>3</sup>, Yung-Kang Peng<sup>2</sup>, Shien-Ping Feng<sup>1,\*</sup>**

<sup>1</sup>Department of Systems Engineering, City University of Hong Kong, Hong Kong 999077, China.

<sup>2</sup>Department of Chemistry, City University of Hong Kong, Hong Kong 999077, China.

<sup>3</sup>Doctech HK Limited, Hong Kong Science Park, Hong Kong 999077, China.

**\*Correspondence to:** Prof. Shien-Ping Feng, Department of Systems Engineering, City University of Hong Kong, Tat Chee Avenue, Kowloon, Hong Kong 999077, China.  
E-mail: [tony.feng@cityu.edu.hk](mailto:tony.feng@cityu.edu.hk)

## Supplementary Note 1

Thermopower enhanced by the establishment of concentration gradients of the redox couple.

In a thermocell, the redox reaction can be expressed as



The thermopower (or Seebeck coefficient) of thermocells describing the essential ability to generate the thermovoltage under a temperature gradient is defined as

$$S_e = \frac{E_{hot} - E_{cold}}{T_{hot} - T_{cold}} = \frac{\Delta S}{nF} = \frac{S_{Ox} - S_{Red}}{nF} \quad (S2)$$

where  $S_e$  is the thermopower,  $E_{hot}$  and  $E_{cold}$  are potential at hot electrode with temperature  $T_{hot}$ , and cold electrode with temperature  $T_{cold}$ , respectively.  $\Delta S$  is the redox reaction entropy change between the entropy of the oxidized ( $S_{Ox}$ ) and reduced species ( $S_{Red}$ ),  $n$  is the number of electrons transferred, and  $F$  is Faraday's constant. According to the Nernst equation, the equilibrium potential ( $E$ ) of the redox reaction in the thermocells can be expressed as

$$E = E^0 + \frac{RT}{nF} \ln \frac{(\alpha_A)^a}{(\alpha_B)^b} \quad (S3)$$

where  $E^0$  is the standard potential,  $\alpha_A$  and  $\alpha_B$  are the chemical activities of the oxidant A and reductant B, respectively, and  $R$  is the ideal gas constant.

The activity of a species in a solution can be expressed as the product of the activity coefficient ( $\gamma_i$ ) and the concentration ( $c_i$ ) of the species ( $\alpha_i = \gamma_i \times c_i$ ). Thus,

Supplementary Equation (S3) can be written as

$$E = E^0 + \frac{RT}{nF} \left[ \ln \frac{(\gamma_A)^a}{(\gamma_B)^b} + \ln \frac{(c_A)^a}{(c_B)^b} \right] \quad (S4)$$

Hence,  $S_e$  in Supplementary Equation (S2) can be rewritten as

$$S_e = \frac{R}{nF(T_{hot} - T_{cold})} \left[ T_{hot} \ln \frac{(\gamma_A)_{hot}^a}{(\gamma_B)_{hot}^b} - T_{cold} \ln \frac{(\gamma_A)_{cold}^a}{(\gamma_B)_{cold}^b} \right] + \frac{R}{nF(T_{hot} - T_{cold})} \left[ T_{hot} \ln \frac{(c_A)_{hot}^a}{(c_B)_{hot}^b} - T_{cold} \ln \frac{(c_A)_{cold}^a}{(c_B)_{cold}^b} \right] \quad (S5)$$

in which the first term containing the activity coefficient ( $\gamma$ ) is dominated by the solvent-dependent entropy difference ( $\Delta S$ ) between the redox ions, and the second term in the equation is related to the concentration difference ( $\Delta C$ ) of the redox ions at two electrodes respectively.

In the liquid-state thermocells,  $\Delta C$  between the redox ions is thermodynamically unstable, and the spontaneous diffusion of the redox ions results in a homogeneous state with  $\Delta C$  near zero. In the pristine  $[\text{Fe}(\text{CN})_6]^{3-/4-}$ -based thermocells, the second term in Supplementary Equation (S5) thus can be neglected. The thermopower only related to  $\Delta S$  is regarded as a constant (the sign of the thermopower is considered here for the discussion of the change), the average value of which is  $-1.21 \text{ mV K}^{-1}$  in our experiment. However, when the additives are introduced into the  $[\text{Fe}(\text{CN})_6]^{3-/4-}$ -based electrolyte system and the corresponding concentration difference profiles are tuned, the second term related to the concentration difference in Supplementary Equation (S5) cannot be neglected anymore ( $\Delta C \neq 0$ ). Hence,  $S_e$  in our thermocell system can be expressed as

$$S_e = -1.21 - \frac{R}{F(T_{hot} - T_{cold})} \left[ T_{hot} \ln \frac{(c_{[\text{Fe}(\text{CN})_6]^{4-}})_{hot}}{(c_{[\text{Fe}(\text{CN})_6]^{3-}})_{hot}} - T_{cold} \ln \frac{(c_{[\text{Fe}(\text{CN})_6]^{4-}})_{cold}}{(c_{[\text{Fe}(\text{CN})_6]^{3-}})_{cold}} \right] \quad (\text{S6})$$

The equation elucidates that  $S_e$  can be enhanced by modulating the concentration difference profiles of the redox ions at two electrodes. More specifically, in our GdnHCl-CH-co-regulated thermocells, the introduction of GdnHCl results in the lower concentrations of  $[\text{Fe}(\text{CN})_6]^{4-}$  at the cold side and the corresponding high concentration of  $[\text{Fe}(\text{CN})_6]^{4-}$  at the hot side, and the addition of CH contributes to a lower concentration of  $[\text{Fe}(\text{CN})_6]^{3-}$  and the corresponding high concentration of  $[\text{Fe}(\text{CN})_6]^{4-}$  at the hot side. Thus,  $S_e$  is increased.

### Supplementary Note 2

Calculation of the thermoelectric properties of thermocells.

For thermocells, the electrical power output can be obtained from the I-V curve from linear sweep voltammetry (LSV). When the I-V curve is nearly linear, the maximum power output ( $P_{max}$ ) can be calculated as

$$P_{max} = \frac{1}{4} V_{oc} I_{sc} \quad (\text{S7})$$

where  $V_{oc}$  is the open-circuit voltage and  $I_{sc}$  is the short-circuit current.

Since thermocells work under temperature gradients, there is heat input power ( $P_{heat}$ ) for maintaining the temperature difference at two electrodes, that is, the thermal power

## Energy Materials

flowing through the cell to maintain the temperature bias. According to the heat-transfer equation,  $P_{heat}$  can be calculated as

$$P_{heat} = \kappa A \frac{\Delta T}{d} \quad (S8)$$

where  $\kappa$  is the thermal conductivity measured,  $A$  is the cross-sectional area of the cell,  $\Delta T$  is the temperature difference between the hot and cold electrodes ( $\Delta T = T_{hot} - T_{cold}$ ), and  $d$  is the distance between the two electrodes. As discussed in the main text, there are thermal conduction and thermal convection involved in the liquid-state thermocells under temperature differences, thus the steady-state method is an appropriate method for measuring the thermal conductivity.

The energy conversion efficiency ( $\eta$ ) is expressed as the ratio of the maximum electrical energy power ( $P_{max}$ ) to the heat input power ( $P_{heat}$ ) as,

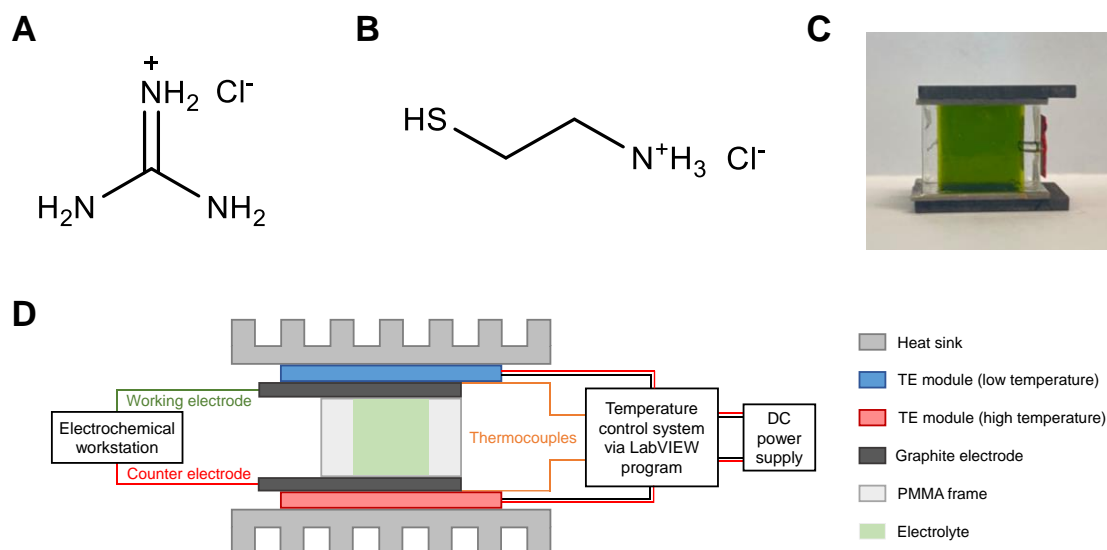
$$\eta = \frac{P_{max}}{P_{heat}} = \frac{1/4 V_{oc} I_{sc}}{\kappa A \Delta T} \cdot d \quad (S9)$$

The Carnot efficiency ( $\eta_c$ ) is known as the limiting efficiency for a heat engine. For the thermocells, it can be expressed as,

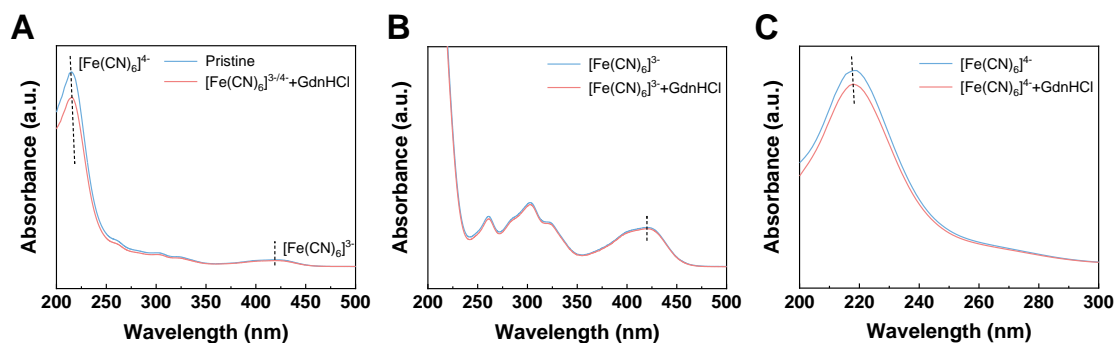
$$\eta_c = \frac{\Delta T}{T_{hot}} \quad (S10)$$

In thermocells, we use the Carnot-relative efficiency ( $\eta_{cr}$ ) to evaluate the performance of a thermocell, which is defined as the ratio of the energy conversion efficiency ( $\eta$ ) of the thermocell to the Carnot efficiency ( $\eta_c$ ),

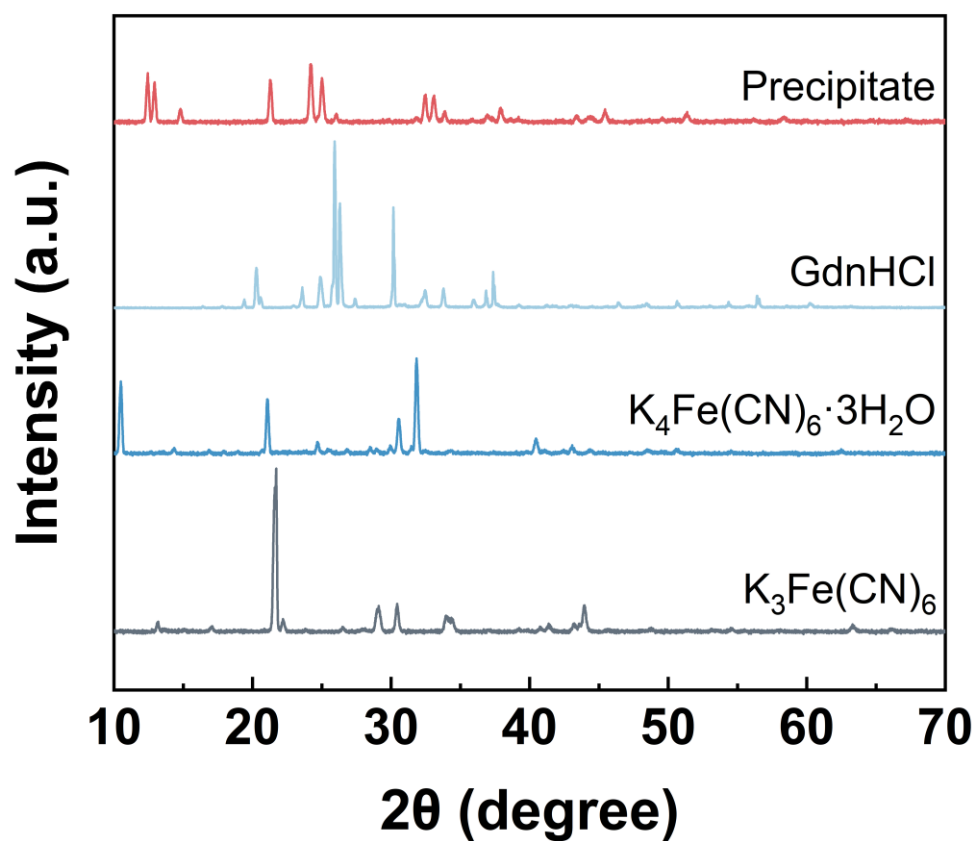
$$\eta_{cr} = \frac{\eta}{\eta_c} \quad (S11)$$



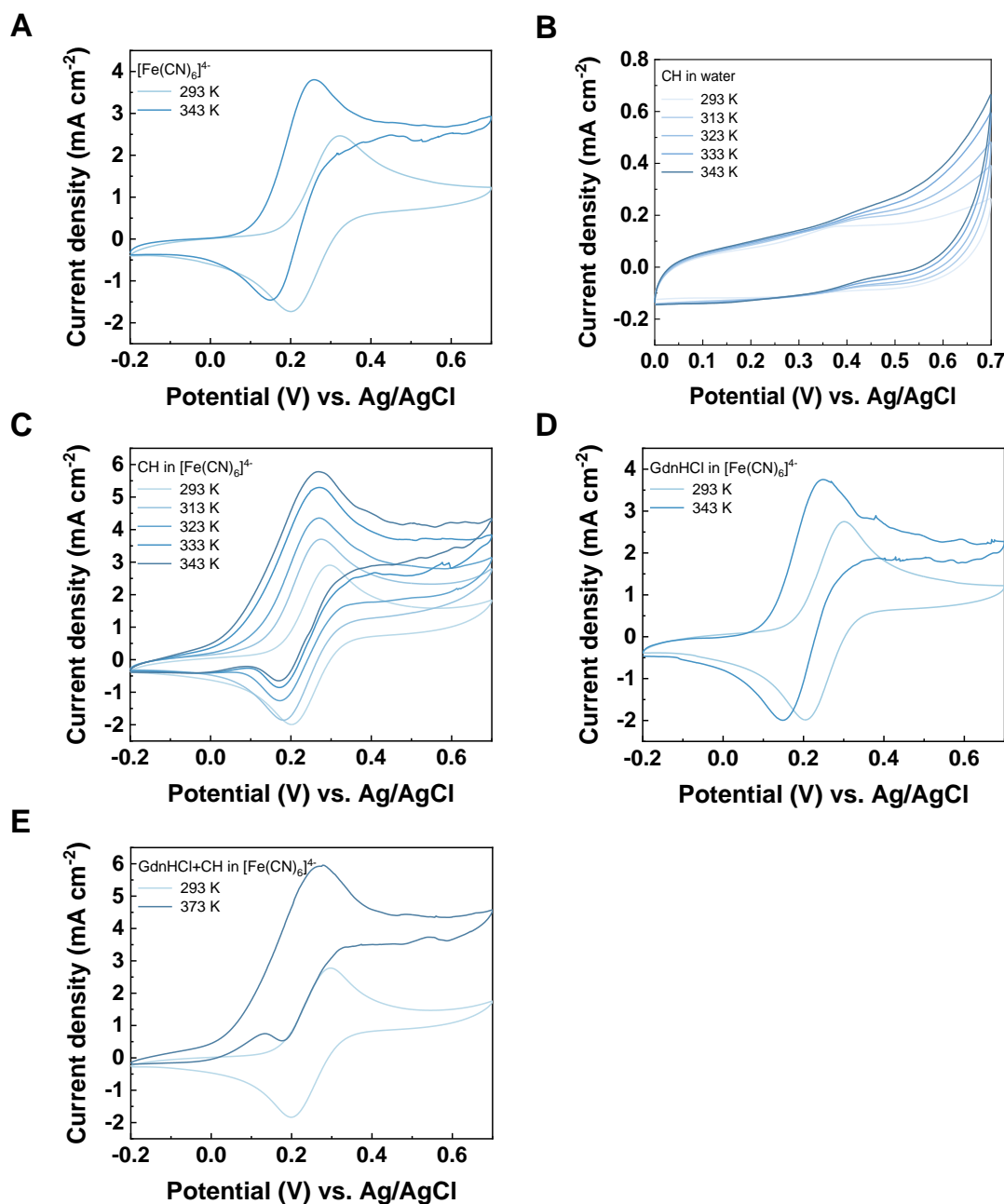
**Supplementary Figure 1.** (A) Chemical structures of guanidine hydrochloride (GdnHCl). (B) Chemical structures of cysteamine hydrochloride (CH). (C) Photograph of a GCTC. The cross-sectional area of the cell is 2.25 cm<sup>2</sup>, and the distance between the two electrodes is 1.5 cm. (D) Experimental setup for thermopower measurement.



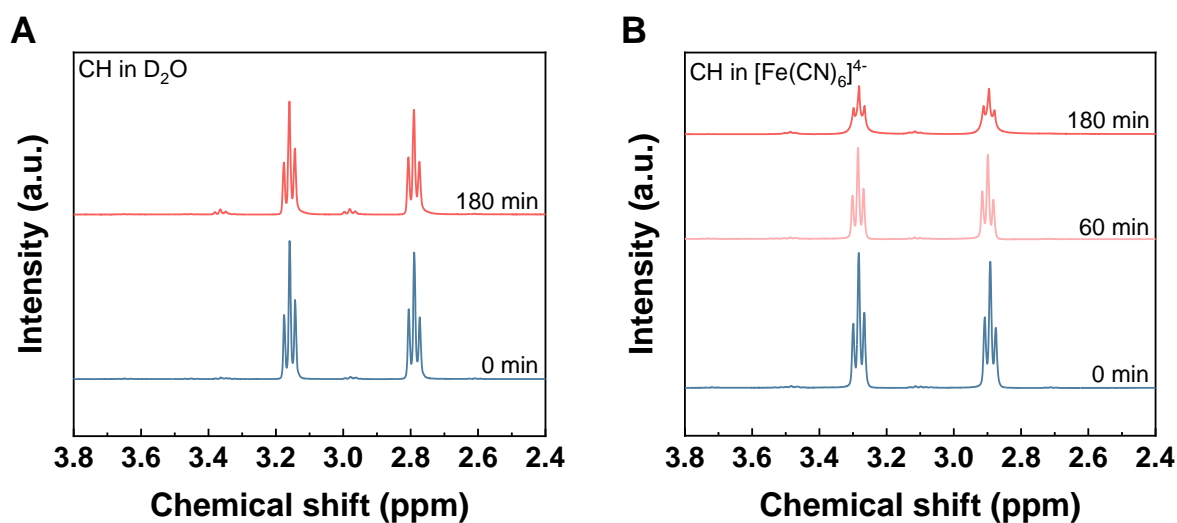
**Supplementary Figure 2.** UV-Vis spectra of (A) [Fe(CN)<sub>6</sub>]<sup>3-/4-</sup> pristine electrolyte, (B) [Fe(CN)<sub>6</sub>]<sup>3-</sup>, and (C) [Fe(CN)<sub>6</sub>]<sup>4-</sup> electrolytes with/without the addition of GdnHCl. The characteristic absorption peaks of [Fe(CN)<sub>6</sub>]<sup>4-</sup> and [Fe(CN)<sub>6</sub>]<sup>3-</sup> are at 218 nm and 420 nm, respectively.



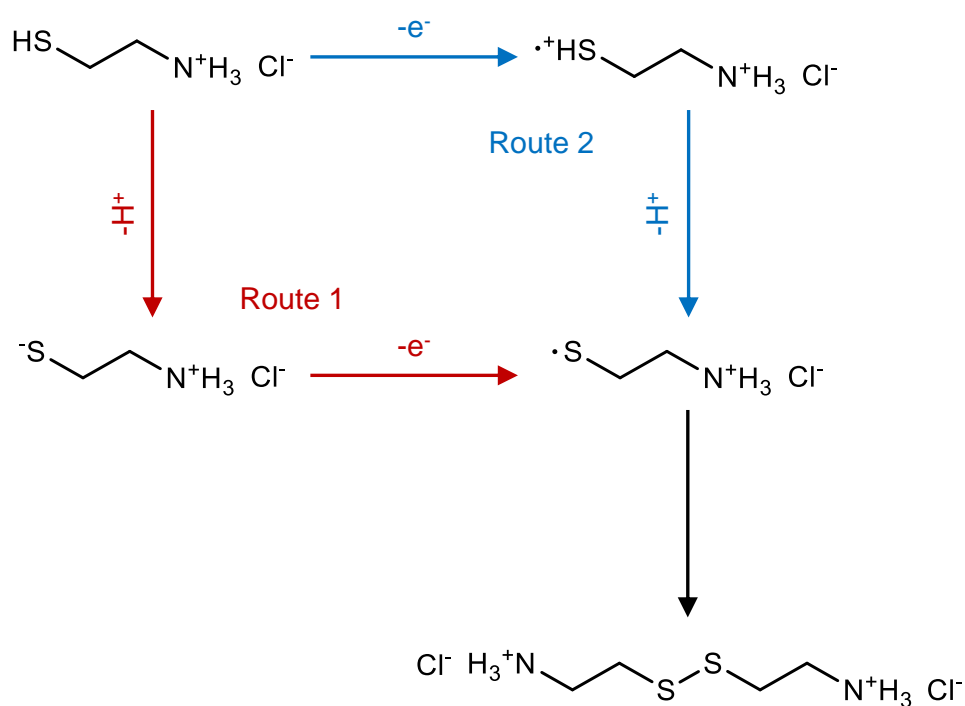
**Supplementary Figure 3.** XRD spectra for pure K<sub>3</sub>Fe(CN)<sub>6</sub>, K<sub>4</sub>Fe(CN)<sub>6</sub>, GdnHCl, and dried powders from the precipitates in the electrolyte with GdnHCl and CH additives.



**Supplementary Figure 4.** Cyclic voltammetry (CV) curves of (A) [Fe(CN)<sub>6</sub>]<sup>4-</sup>, (B) CH, and [Fe(CN)<sub>6</sub>]<sup>4-</sup> electrolyte with additives of (C) CH, (D) GdnHCl, and (E) GdnHCl and CH, at different temperatures. The concentrations of [Fe(CN)<sub>6</sub>]<sup>4-</sup> in all CV analyses were 0.02 M with 0.5 M KCl as the supporting electrolyte. All CV analyses adopted graphite sheet (with a size of 1×1 cm<sup>2</sup>) as the working electrode, Pt (with a size of 0.5×2 cm<sup>2</sup>) as the counter electrode, and Ag/AgCl in saturated KCl solution as the reference electrode. The scan rate was 10 mV s<sup>-1</sup>.

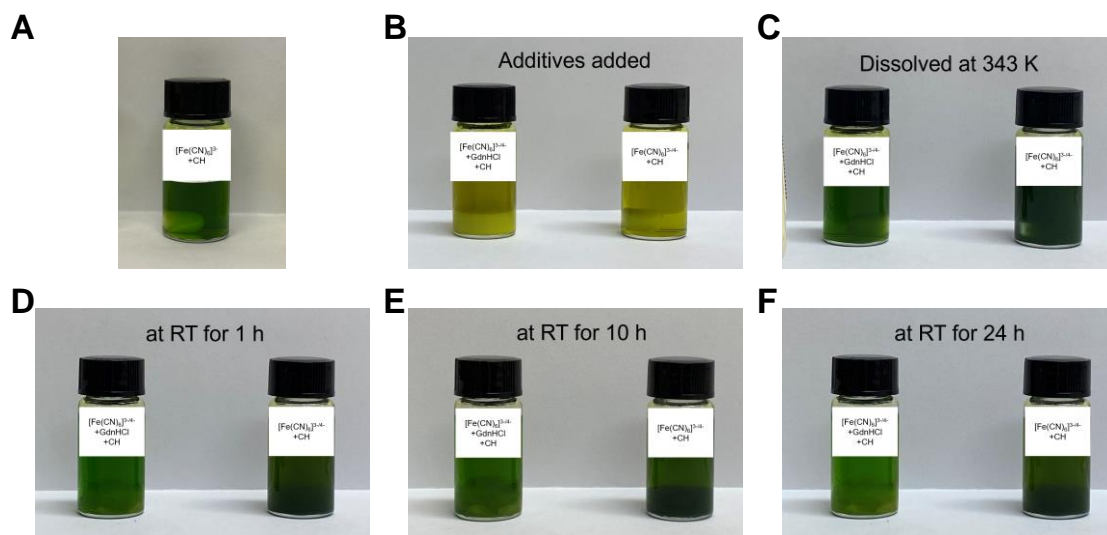


**Supplementary Figure 5.**  $^1\text{H}$  NMR spectra of evolution of CH in (A)  $\text{D}_2\text{O}$ , and (B)  $[\text{Fe}(\text{CN})_6]^{4-}$  electrolyte at 343 K.

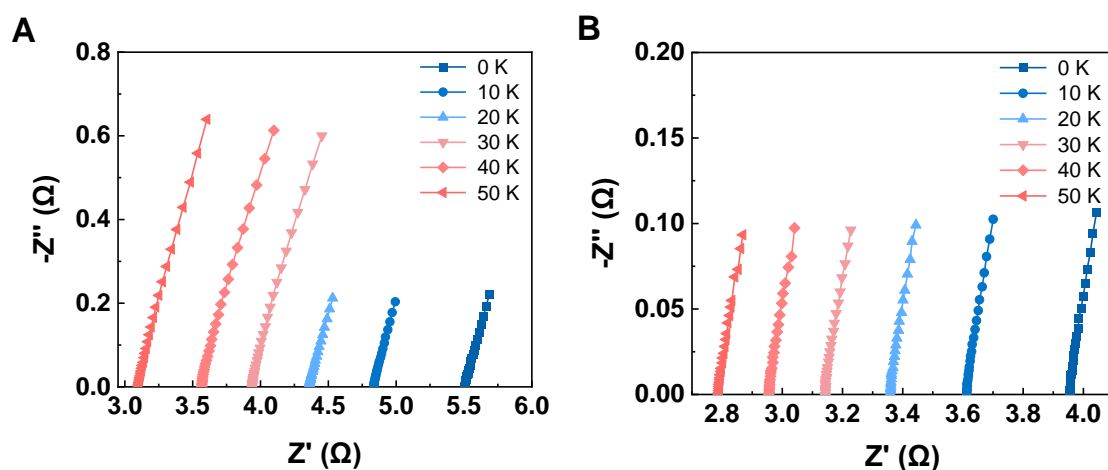


**Supplementary Figure 6.** Schematic of two possible mechanistic pathways for the oxidation of CH to CDH.

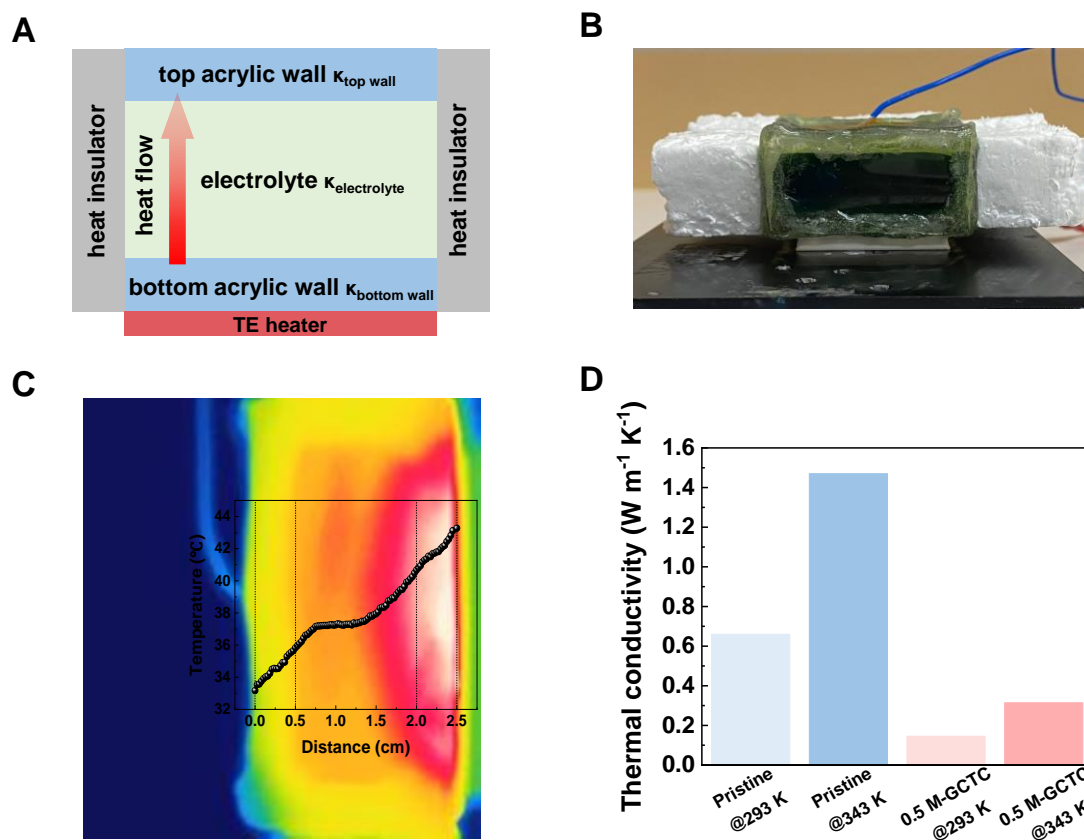




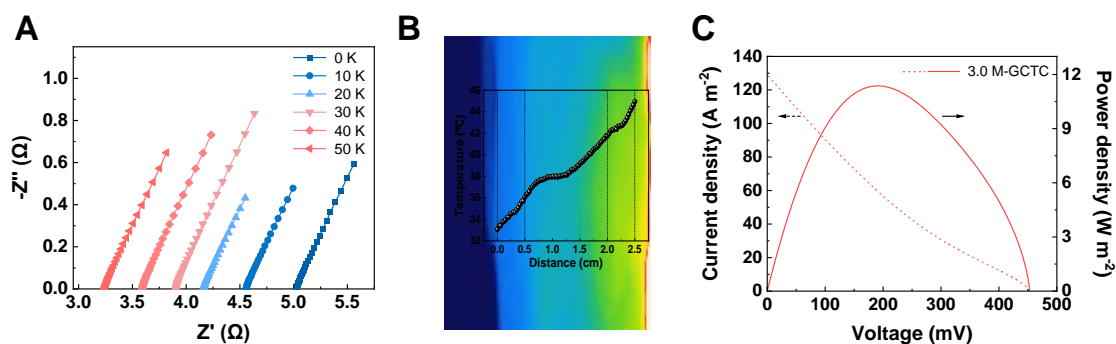
**Supplementary Figure 7.** (A) Photograph of  $[\text{Fe}(\text{CN})_6]^{3-}$  with sole CH additive dissolved at 343 K. For CH directly interacting with  $[\text{Fe}(\text{CN})_6]^{3-}$ , a clear green color was presented. (B-F) Photographs of the color evolution of  $[\text{Fe}(\text{CN})_6]^{3-/4-}$ -CH electrolyte with (left)/without (right) the addition of GdnHCl. (B) Initial addition of GdnHCl and CH into the left  $[\text{Fe}(\text{CN})_6]^{3-/4-}$  electrolyte, and sole CH into the right  $[\text{Fe}(\text{CN})_6]^{3-/4-}$  electrolyte. (C) Both solutions were heated at 343 K for the dissolution of additives. After dissolution, the solutions were placed at room temperature for (D) 1 h, (E) 10 h, and (F) 24 h. When the additives were introduced into the  $[\text{Fe}(\text{CN})_6]^{3-/4-}$  electrolyte, the colors of both electrolytes were similar. After the additives dissolved, a clear green color was found in the left  $[\text{Fe}(\text{CN})_6]^{3-/4-}$  electrolyte with GdnHCl and CH as the additives over time, which is similar to that of sole CH in  $[\text{Fe}(\text{CN})_6]^{3-}$ , while the right one without GdnHCl showed a different dark green color.



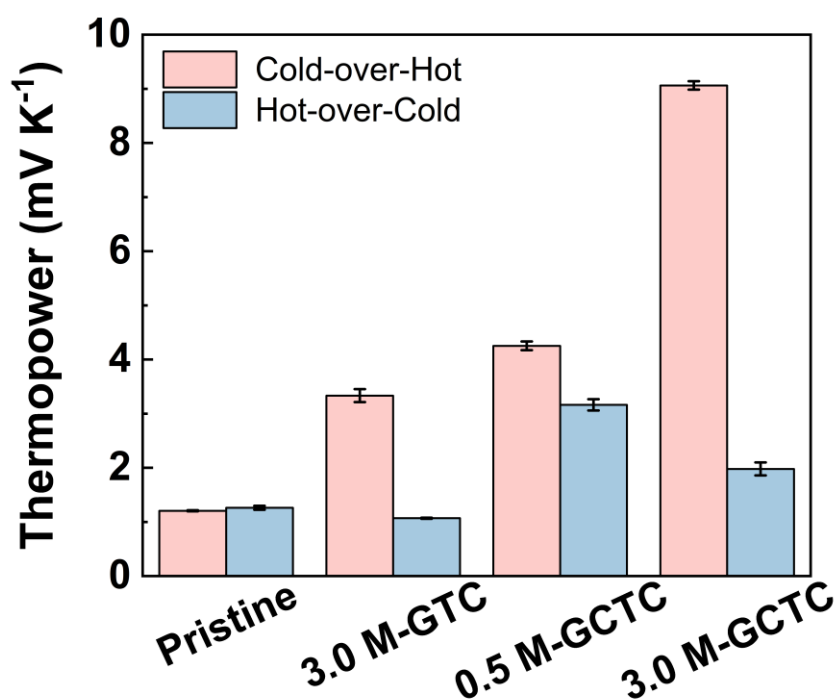
**Supplementary Figure 8.** Electrochemical impedance spectra of (A) 0.5 M-GCTC, and (B) pristine thermocell containing 0.4 M  $[\text{Fe}(\text{CN})_6]^{3-/4-}$  electrolyte without additives, at varying temperature differences from 0 to 50 K.



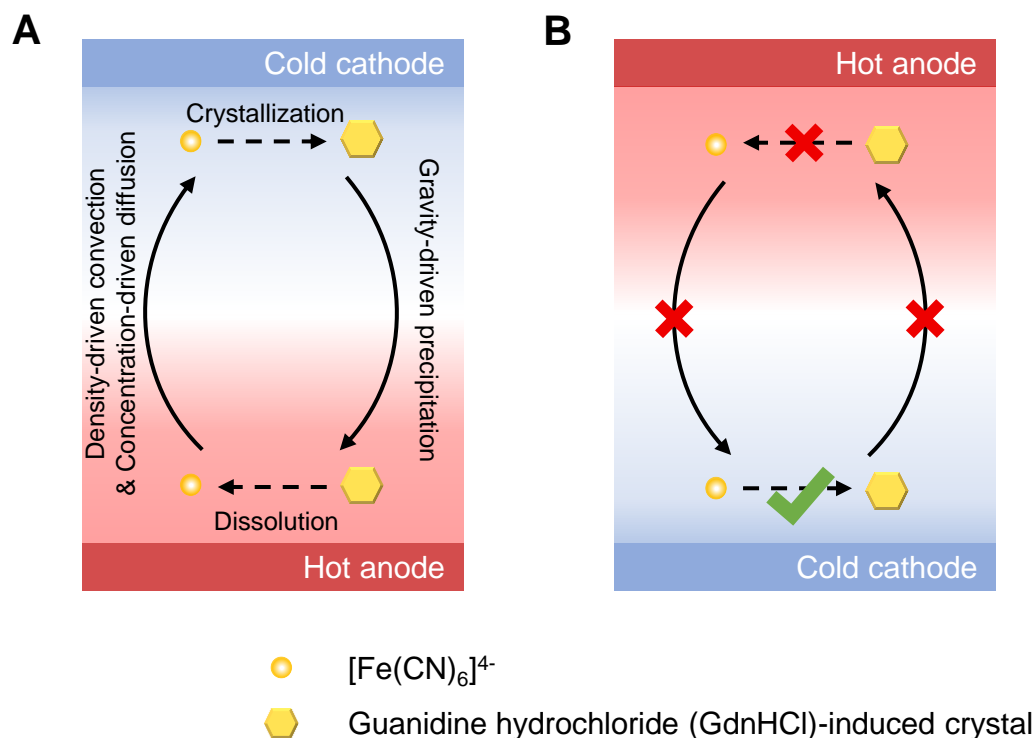
**Supplementary Figure 9.** Thermal conductivity analysis. (A) Schematic, and (B) digital image of the devised device for the thermal conductivity measurement via the steady-state method. (C) Infrared thermography image and corresponding temperature profile within the device. To facilitate temperature profile interpretation, the infrared thermography image is rotated  $90^{\circ}$  counterclockwise. (D) The thermal conductivity of the pristine thermocell and 0.5 M-GCTC.



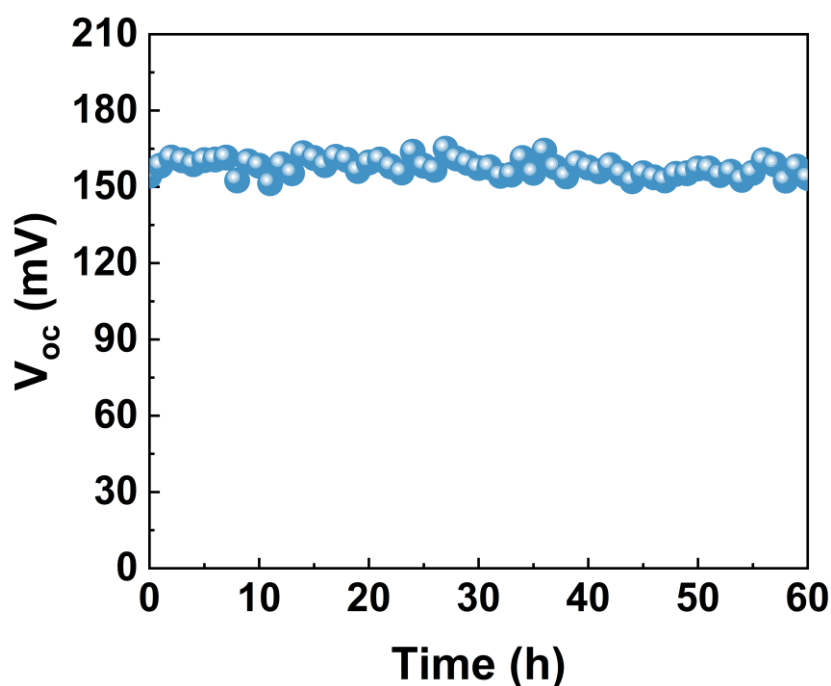
**Supplementary Figure 10.** Thermoelectric performance of 3.0 M-GCTC with optimal concentrations for GdnHCl and CH at 3.0 M and 50 mg mL<sup>-1</sup>, respectively. (A) Electrochemical impedance spectra at varying temperature differences from 0 to 50 K. (B) Infrared thermography image and corresponding temperature profile within 3.0 M-GCTC. (C) Current density versus thermovoltage and corresponding power density.



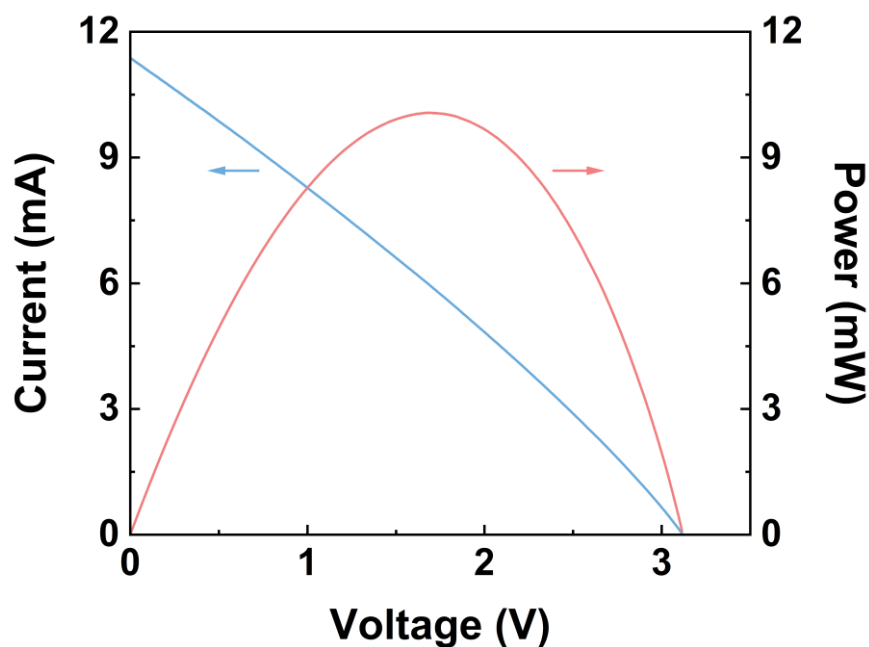
**Supplementary Figure 11.** Dependence of thermopower values on the cell orientations in pristine thermocell, 3.0 M-GTC, 0.5 M-GCTC, and 3.0 M-GCTC.



**Supplementary Figure 12.** Schematic of the high orientation dependence of GdnHCl-added thermocells. (A) Thermosensitive crystallization and redissolution cycle of  $[\text{Fe}(\text{CN})_6]^{4-}$  induced by GdnHCl additive under the cold-over-hot orientation. Crystals formed via the selective crystallization interaction between GdnHCl and  $[\text{Fe}(\text{CN})_6]^{4-}$  accomplish the cycle within the thermocells by gravity-driven precipitation of the crystals from the top cold side to the bottom hot side, and the density imbalance-driven convection and concentration gradient-driven diffusion from the bottom to the top after the thermosensitive dissolution of the crystals at elevated temperatures at the bottom hot side. (B) No thermosensitive crystallization and redissolution cycle of  $[\text{Fe}(\text{CN})_6]^{4-}$  induced by GdnHCl additive under the hot-over-cold orientation. The precipitates only accumulate at the bottom cold side, leading to a substantial reduction in the thermoelectric response.



**Supplementary Figure 13.** The open-circuit voltage ( $V_{oc}$ ) versus time for 0.5 M-GCTC during a continuous operation of 60 hours at a  $dT$  of 40 K. The temperature of cold side was controlled at  $\sim 293$  K.



**Supplementary Figure 14.** Current versus thermovoltage and corresponding power output of the GCTC module in the hot-over-cold arrangement at a  $\Delta T$  of 50 K. The module contained 20 units of 0.5 M-GCTCs connected in series.

**Supplementary Table 1. Comparison of the  $S_e$  and  $\eta_{cr}$  of our GCTC system with other reported  $[\text{Fe}(\text{CN})_6]^{3-/4-}$ -based thermocells. The values (\*) not directly given in the corresponding literature were retrieved from figures or calculated based on the given parameters using Supplementary Equation (S11)**

Optimization	Electrolyte	Electrode	T <sub>cold</sub> (K)	T <sub>hot</sub> (K)	$S_e$ (mV K <sup>-1</sup> )	$\eta_{cr}$ (%)	Ref.
Electrolyte	0.4 M $\text{K}_3\text{Fe}(\text{CN})_6$ / $\text{K}_4\text{Fe}(\text{CN})_6$ +0.5 M GdnHCl +50 mg mL <sup>-1</sup> CH	Graphite	293	343	4.34	5.50	This work
	0.4 M $\text{K}_3\text{Fe}(\text{CN})_6$ / $\text{K}_4\text{Fe}(\text{CN})_6$ +3.0 M GdnHCl +50 mg mL <sup>-1</sup> CH	Graphite	293	343	9.06	12.65	
	0.4 M $\text{K}_3\text{Fe}(\text{CN})_6$ / $\text{K}_4\text{Fe}(\text{CN})_6$ +3.0 M <sup>a</sup> GdmCl	Graphite	293	343	3.73	3.86*	26
	0.4 M $\text{K}_3\text{Fe}(\text{CN})_6$ / $\text{K}_4\text{Fe}(\text{CN})_6$ +2.6 M GdmCl	Graphite	293	303	2.7	0.34	25
	0.4 M $\text{K}_3\text{Fe}(\text{CN})_6$ / $\text{K}_4\text{Fe}(\text{CN})_6$ +2.6 M GdmCl +24 M Urea	Graphite	293	303	4.2	0.79	

Electrode	0.4 M K <sub>3</sub> Fe(CN) <sub>6</sub> /K <sub>4</sub> Fe(CN) <sub>6</sub>	<sup>b</sup> MWNT buckypaper	278	338	1.4	1.4	41
	0.4 M K <sub>3</sub> Fe(CN) <sub>6</sub> /K <sub>4</sub> Fe(CN) <sub>6</sub>	<sup>c</sup> SWNT-rGO composite (single)	343*	374*	1.42	0.65*	38
	0.4 M K <sub>3</sub> Fe(CN) <sub>6</sub> /K <sub>4</sub> Fe(CN) <sub>6</sub>	SWNT-rGO composite (10-stack)	343*	374*	1.42	2.63	
	0.4 M K <sub>3</sub> Fe(CN) <sub>6</sub> /K <sub>4</sub> Fe(CN) <sub>6</sub>	<sup>d</sup> CNT aerogel sheet	303	373	1.43	3.95	42
	0.4 M K <sub>3</sub> Fe(CN) <sub>6</sub> /K <sub>4</sub> Fe(CN) <sub>6</sub>	MWNT	273	313	1.42	0.9	43
	0.9 M K <sub>3</sub> Fe(CN) <sub>6</sub> / (NH <sub>4</sub> ) <sub>4</sub> Fe(CN) <sub>6</sub>	Activated carbon cloth (with thermal separator)	274	373	1.43	0.4	44
Electrolyte +Electrode	0.4 M K <sub>3</sub> Fe(CN) <sub>6</sub> /K <sub>4</sub> Fe(CN) <sub>6</sub> + Formamide (FA:H <sub>2</sub> O, 1:1)	Anisotropic holey graphene oxide	233	373	1.3	0.7	45
	0.4 M K <sub>3</sub> Fe(CN) <sub>6</sub> /K <sub>4</sub> Fe(CN) <sub>6</sub> +3.0 M GdmCl	Carbon fabric paper+graphite	293	333	3.73	11.1	26

Note: <sup>a</sup>GdmCl: guanidinium chloride; <sup>b</sup>MWNT: multiwalled carbon nanotube <sup>c</sup>SWNT-rGO: single walled carbon nanotube-reduced graphene oxide; <sup>d</sup>CNT: carbon nanotube.

**Supplementary Table 2. Comparison of liquid-state thermocells and thermoelectric materials on methodologies of thermoelectric performance analysis widely employed**

Thermoelectric factor	Liquid-state thermocells	Ref.	Thermoelectric semiconductor materials	Ref.
Thermopower	<u>Principle:</u> $S = \frac{\Delta V}{\Delta T}$ <p>Measure the open-circuit voltage <math>V_{oc}</math> under temperature difference steps <math>\Delta T</math> and retrieve the slope of <math>V_{oc}</math>-<math>\Delta T</math>.</p>	24	<u>Principle:</u> $S_e = -\frac{\Delta V}{\Delta T}$ <p>Measure the open-circuit voltage <math>V_{oc}</math> under temperature difference steps <math>\Delta T</math> and retrieve the slope of <math>V_{oc}</math>-<math>\Delta T</math>.</p>	9, 46
	<u>Method:</u> <p>Two thermoelectric modules or circulating water bath accompanied with two K-type thermocouples for temperature control;            Potentiostat/ Galvanostat, electrochemical</p>		<u>Method:</u> <p>Commercial measurement system (e.g. Netzsch SBA 458 and ULVAC-RIKO ZEM-3).</p>	



workstation or SourceMeter for voltage recording.

Principle:

$$\sigma = l/(R \cdot S)$$

Measure the resistance ( $R$ ) to calculate electrical conductivity  $\sigma$  with electrode separation ( $l$ ) and contact area ( $S$ ).

Principle:

$$\sigma = l/(R \cdot S)$$

Measure the resistance ( $R$ ) to calculate electrical conductivity  $\sigma$  with electrode separation ( $l$ ) and contact area ( $S$ ).

Electrical  
conductivity

Method:

- a. Electrochemical impedance spectroscopy (EIS) via Potentiostat/Galvanostat or electrochemical workstation; high frequency  $x$ -axis intercept value in Nuiquist plot as the resistance.
- b. Linear sweep voltammetry (LSV) via Potentiostat/Galvanostat or electrochemical

26, 42, 44

Method:

Commercial measurement system that measures the thermopower (Seebeck coefficient) and electrical conductivity simultaneously; resistance obtained from the I-V curve.

9, 46, 47

workstation for I-V characteristic curve;  
slope of I-V curve as the resistance.

Principle:

Based on heat flux conservation law; both  
thermal conduction and convection  
considered.

Principle:

$$\kappa = D\rho C_p$$

Measure thermal diffusivity ( $D$ ), density ( $\rho$ ) and  
heat capacity ( $C_p$ ) to calculate thermal  
conductivity ( $\kappa$ ).

Thermal      Method:  
conductivity      Steady-state method      26

Method:      48, 49

Laser flash method for measurement of thermal  
diffusivity; differential scanning calorimetry  
(DSC) and commercial measurement system for  
high- and low-temperature heat capacity  
measurement, respectively.

## Supplementary Movie 1.

Demonstration of the GCTC module for directly powering various electronic devices, including an electrochromic smart window, a green LED light, and a thermohydrometer.